Supporting Information

A New Strategy Based on Shear-Thinning and Ice-Growth-Inhibition to 3D Printing Lightweight Lamellar Graphene Aerogels for Electromagnetic Interference Shielding and Piezoresistive Sensor Applications

*Hao Guo, Tianxiang Hua, Jing Qin, Qixin Wu, Rui Wang, Bo Qian *, Lingying Li and Xuejun Shi*

This PDF file includes:

Formula S1 to S11

Figures S1 to S16

Table S1 to S3

Other Supplementary Materials for this manuscript include the following:

Videos S1

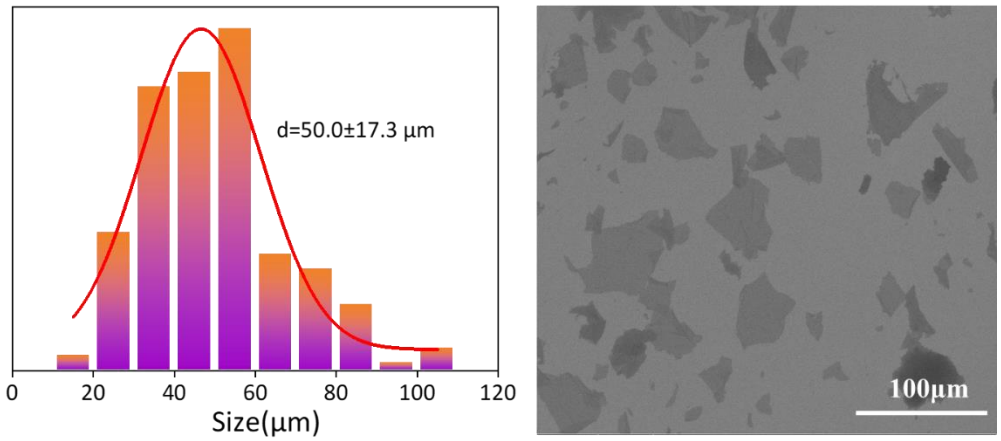

Figure S1. (a) histogram of the sizes of GO sheets. The mean lateral size of GO sheets are around 30μm. (b) SEM of GO sheets.

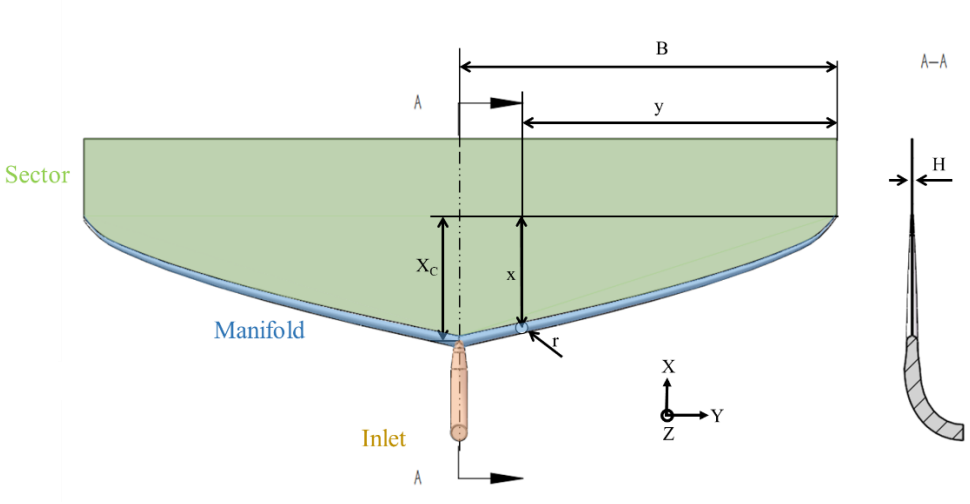

Figure S2. Schematic diagram of coat-hanger die. Front view, central cross-section.

Mathematical formulation of the coat-hanger die[1]

The manifold radius $R(y)$ in y-axis direction expressed as follows:

$$R(y) = m^{\frac{1}{3(n+1)}} \cdot \pi^{-\frac{1}{3}} \cdot \left\{\frac{(3n+1)}{2(2n+1)}\right\}^{\frac{n}{3(n+1)}} \cdot H^{\frac{2}{3}} \cdot (B-y)^{\frac{1}{3}} \tag{S1}$$

Where m is the ratio of residence time in the manifold to residence time in the slot; n is the flow behavior index in the Formula 1; H is the gap of the coat-hanger die section; B is the half of the coat-hanger width.

In our designed coat-hanger die, $m = 1$ according to the assumptions, H sets as 50μm, B sets as 15mm.

The height of manifold to the slot outlet of the

$$x(y) = \int_0^x \mathrm{d}x = \int_0^y \left\{\frac{k'}{(L-y)^{\frac{2}{3}} - k'}\right\}^{\frac{1}{2}} \mathrm{d}y$$

$$= -\frac{3}{2} \cdot k'^{\frac{1}{2}} \left[(L-y)^{\frac{1}{3}} \cdot \sqrt{(L-y)^{\frac{2}{3}} - k'} + k' \ln\left\{(L-y)^{\frac{1}{3}} + \sqrt{(L-y)^{\frac{2}{3}} - k'}\right\}\right]^{y} \tag{S2}$$

Where k' :

$$k' = m^{\frac{-2(3n+1)}{3(n+1)}} (\pi H)^{\frac{2}{3}} \left\{\frac{(3n+1)}{2(2n+1)}\right\}^{\frac{4n}{3(n+1)}}$$

The center height of the coat-hanger die X(0), is calculated as:

$$\mathrm{X}(0) = \int_0^{L-k^2} \left\{\frac{k'}{(L-y)^{2/3} - k'}\right\}^{\frac{1}{2}} \mathrm{d}y$$

$$= -\frac{3}{2} \cdot k^{\frac{1}{2}} \left[k' \log_e k^{\frac{1}{2}} - L^{\frac{1}{3}} \sqrt{L^{2/3} - k'} - k' \ln\left\{L^{\frac{1}{3}} + \sqrt{L^{2/3} - k'}\right\}\right] \tag{S3}$$

Table S1. Power-law parameters (K and n) of GO dispersions and The quantitative

GO dispersions	n	K	B (mm)	H (μm)	$R(0)$ (mm)	$X(0)$ (mm)
GO-T0	0.216	4.10	15	50	0.2212	4.9519
GO-T2	0.248	4.04	15	50	0.2205	4.9191
GO-T4	0.308	3.55	15	50	0.2194	4.8659

parameters of the coat-hanger die

the formula for calculating shear rate of pseudoplastic fluid flow in flat slit:

$$\dot{\gamma}_w = \left(\frac{1+2n}{2n}\right) \cdot \frac{\dot{V}}{B \cdot H^2} = \left(\frac{1+n}{n}\right) \cdot \frac{v}{H} \tag{4}$$

Where $\dot{\gamma}_w$ is the shear rate; n is the flow behavior index in the Formula 7; H is the thickness of the coat-hanger die section; B is the half of the coat-hanger width; $\dot{V}$ is the mean volume flow. v is the fluid velocity in the middle plane.

the velocity of plunger flow:

$$v_h = v \cdot (1 - (\frac{h}{H})^{\frac{n+1}{n}}) \tag{5}$$

Where h is the distance from the middle plane in the slit; v_h is the velocity at different h in the slit.

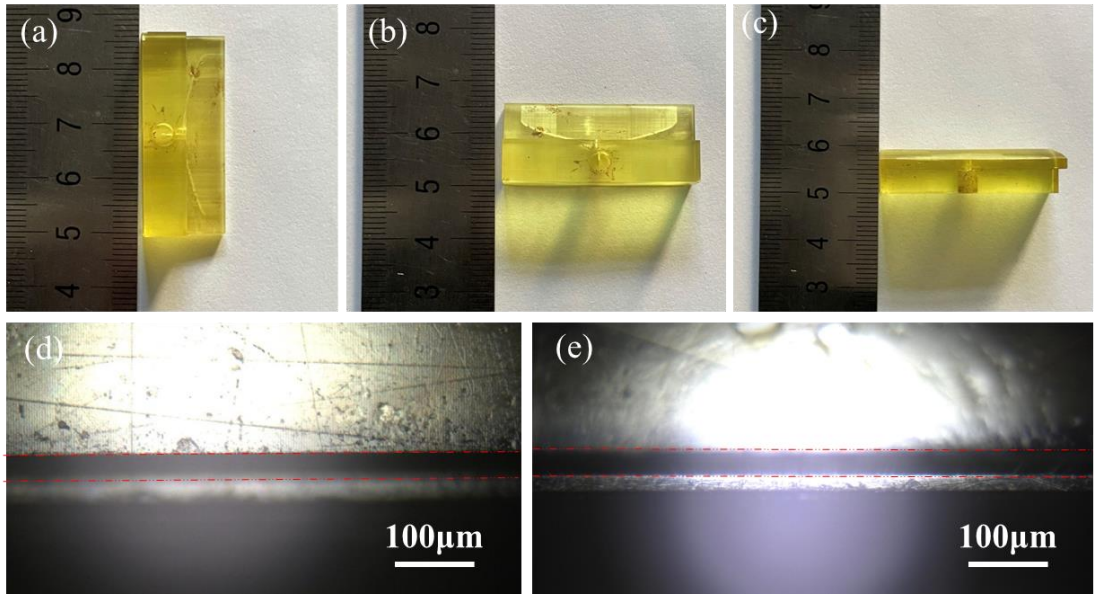

Figure S3.(a-c) Digital photos of the extrusion .(d-e)the optical picture of the slit.

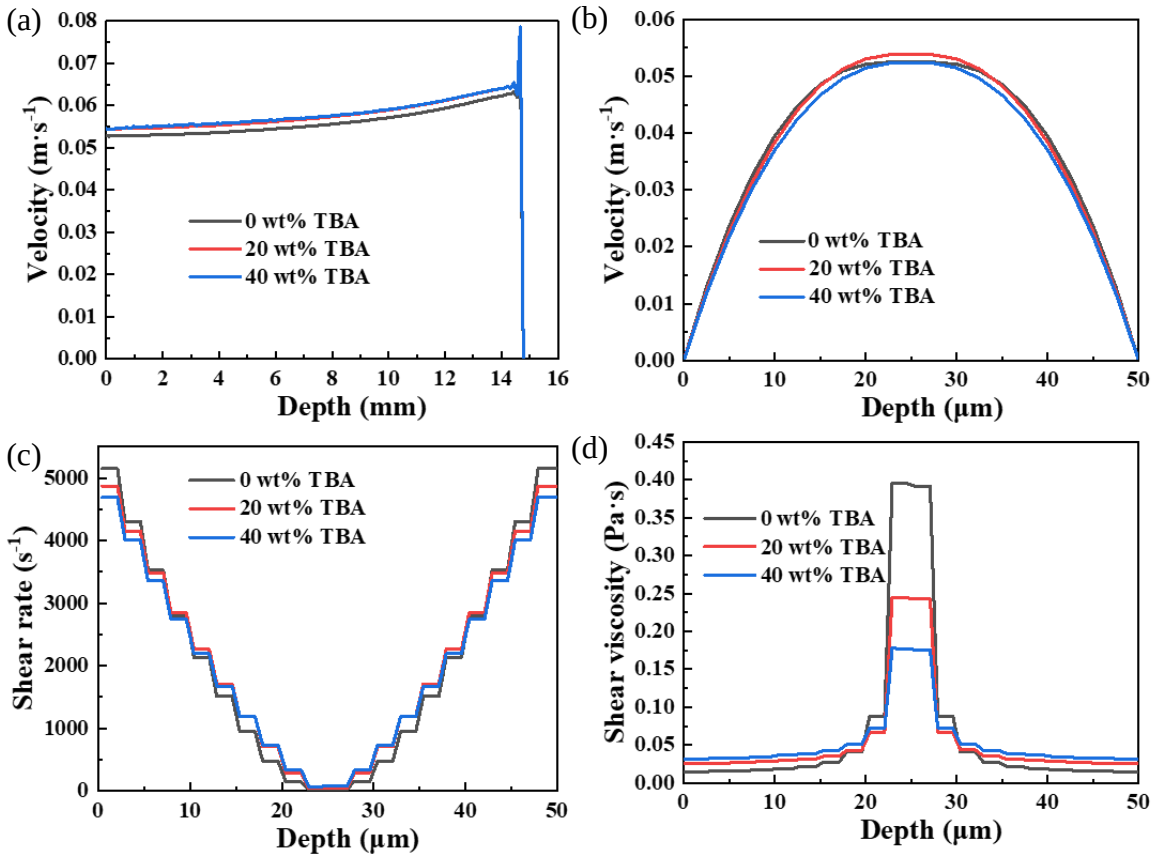

Figure S4. Finite Element Simulation of the GO dispersions at the outlet of the extrusion head channel. Inlet pressure is 50 kPa. Reference table S1 for extrusion head model parameters and Power-law equation parameters. (a) velocity distribution of GO dispersions at the x−y plane of outlet. (b) velocity distribution of GO dispersions at the x−z plane of outlet. (c) Shear rate distribution of GO dispersions at the x−z plane. (c) Shear viscosity distribution of GO dispersions at the x−z plane.

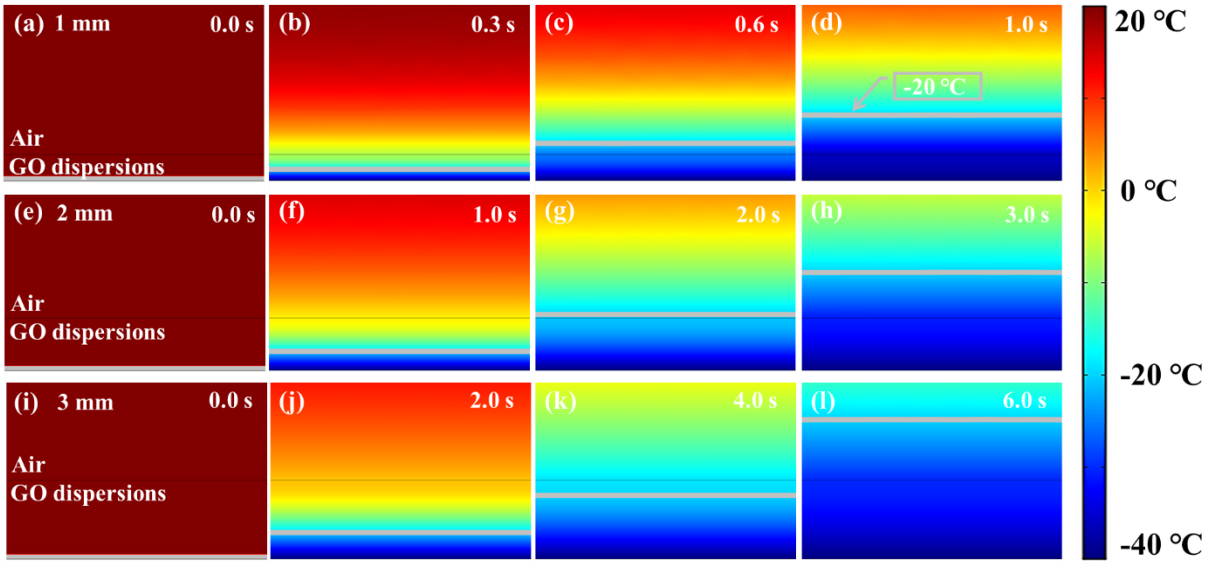

Figure S5. Finite Element Simulation of time dependent temperature distributions of GO-T4 dispersions.(a) 1 mm thickness, (b) 2 mm thickness, (c) 3 mm thickness.

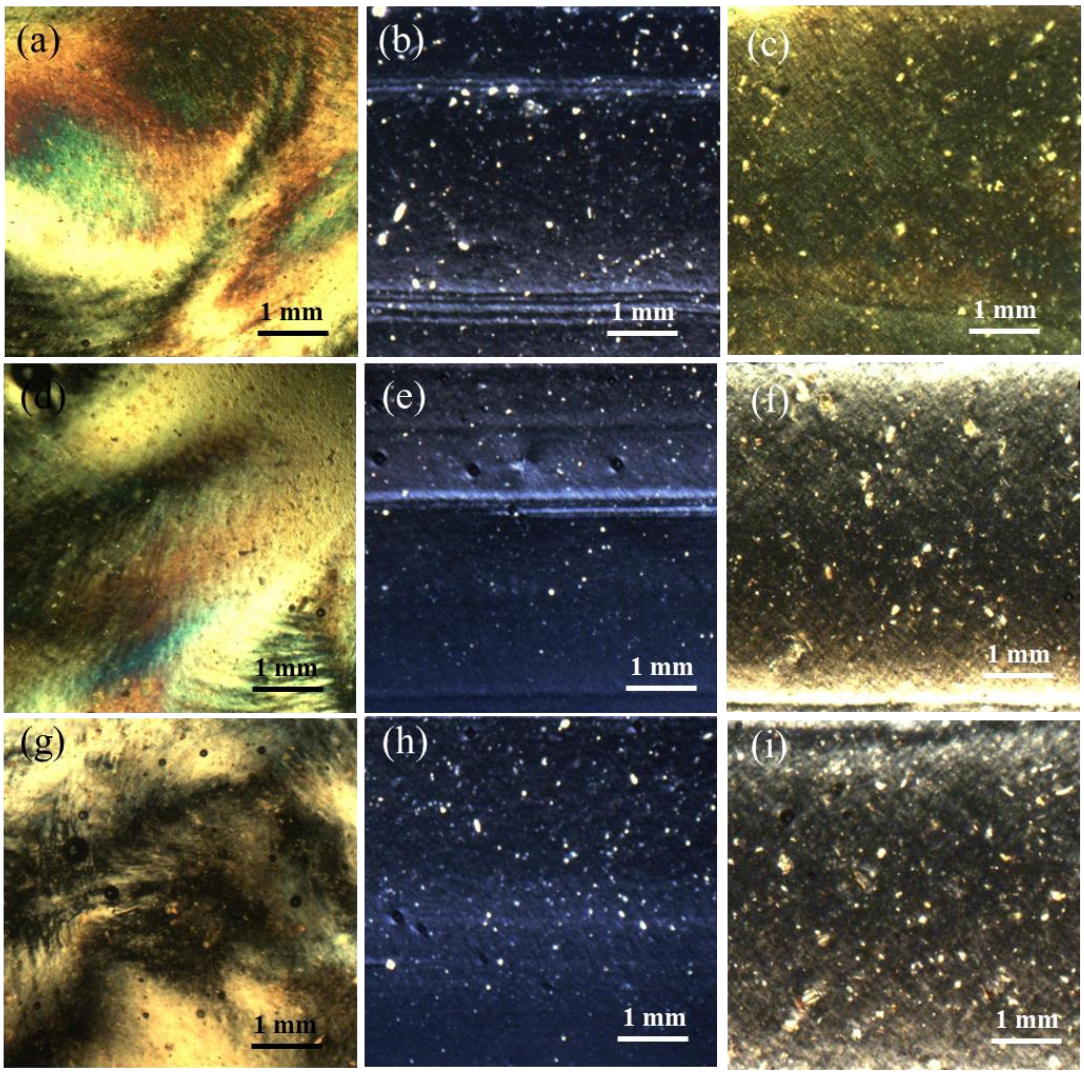

Figure S6. Polarized optical microscope (POM) images of (a-c) GO-T0, (d-f) GO-T2 and (g-i) GO-T4 before extrusion, after extrusion and after multilayer extrusion.

Figure S7. (a)Digital photos of GOA-T4. (b)Digital photos of GA-T4.

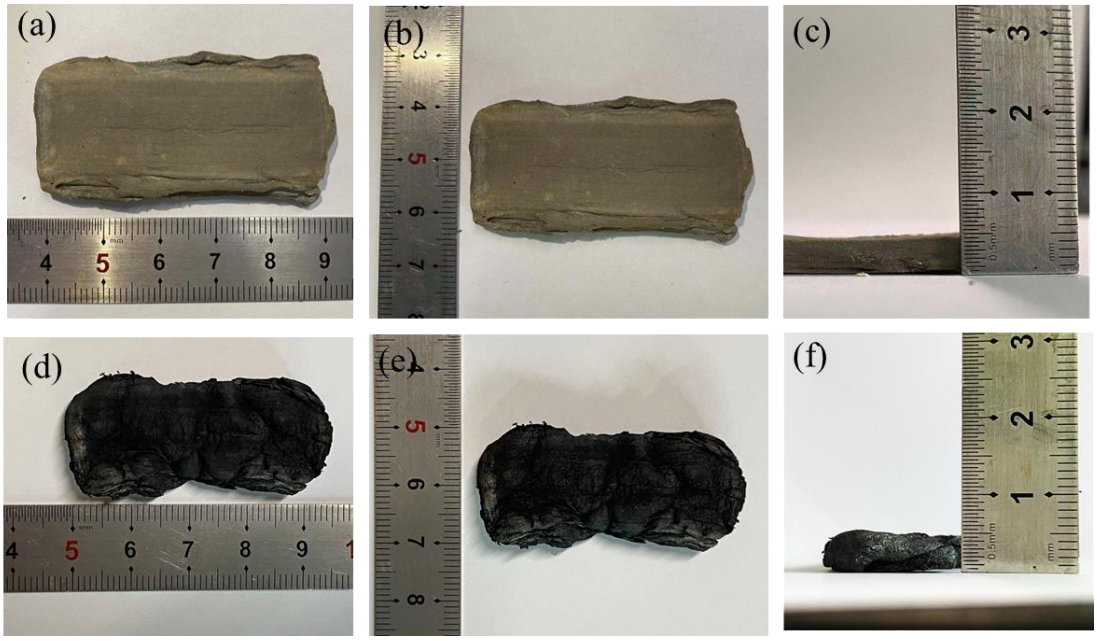

Figure S8. (a-c)Digital photos of GOA-T4. (d-f) Digital photos of GA-T4.

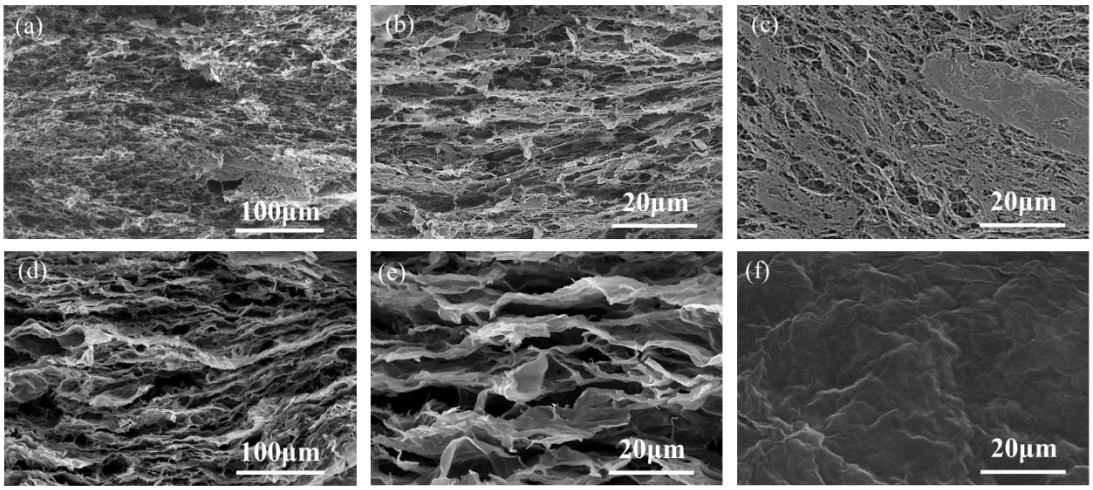

Figure S9. SEM images of GOA-T4 internal morphology in vertical(a,b) and horizontal(c) directions. SEM images of GA-T4 internal morphology in vertical(d,e) and horizontal(f) directions.

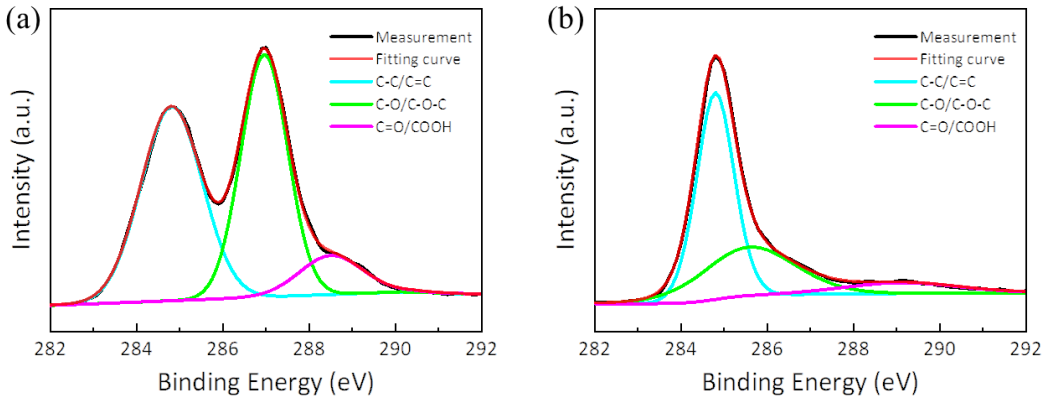

Figure S10.(a-b) High-resolution XPS spectra (C 1s) of (a) GOA-T4 and (b) GA-T4.

Mathematical formulation of the shield efficiency calculate ：

S11 and S21 represent the reflection coefficient and transmission coefficient of the material to the electromagnetic(EM) wave, which are directly obtained by the vector network analyzer. The transmittance (T) and reflectance (R) of the samples are calculated by the following formulas[2]:

$$R = |S11|^2, \quad T = |S21|^2$$

And the absorbance coefficient (A) can be calculated from the follow relationship:

$$A=1-R-T \tag{6}$$

Absorption efficiency is related to the absorbed power of the incident EM wave after entering the material and the residual power of the incident EM wave after reflection. The calculation formula is as follows:

$$A_{eff} = \frac{A}{1-R} = \frac{1-R-T}{1-R} \tag{7}$$

The total EMI SE (SE_T) of a material consists of the contributions from reflection (SE_R), absorption (SE_A) and multiple reflections (SE_M), and their relationship is that:

$$SE_T = SE_R + SE_A + SE_M \tag{8}$$

and SE_M can be ignored in case SE_T> 15 dB, therefore,

$$SE_T(dB) = SE_R(dB) + SE_A(dB) \tag{9}$$

The reflection and absorption shielding effectiveness can be extracted from the following equation:

$$SE_R(dB) = -10 \log (1 - R) \tag{10}$$

and

$$SE_A(dB) = -10 \log(1 - A_{eff}) = -10 \log\left(1 - \frac{1-R-T}{1-R}\right) = -10 \log\left(\frac{T}{1-R}\right) \tag{11}$$

and, Z_{in} is the absorbent input impedance, calculated with the equation:

$$Z_{in} = Z_0\sqrt{\frac{\mu_r}{\varepsilon_r}}thah(j\frac{2\pi f d\sqrt{\mu_r\varepsilon_r}}{c}) \tag{12}$$

where Z_0 is the impedance of air, μ_r is the relative permeability, ε_r is the relative permittivity, j is the imaginary unit of complex number, c is the speed of light, d is the thickness of the sample, and f is the microwave frequency.

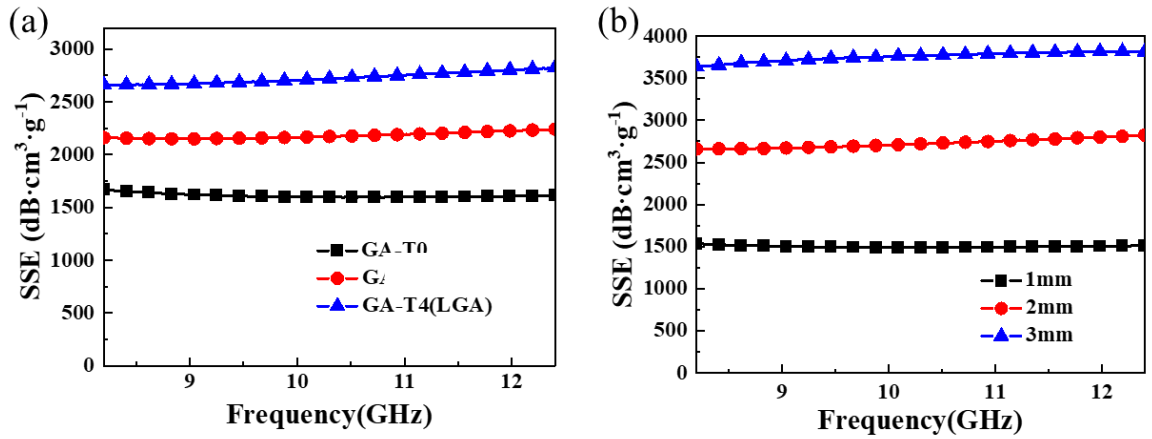

Figure S11. (a) SSE of the GAs with different TBA content. (b)SSE of GA-T4 with different thickness.

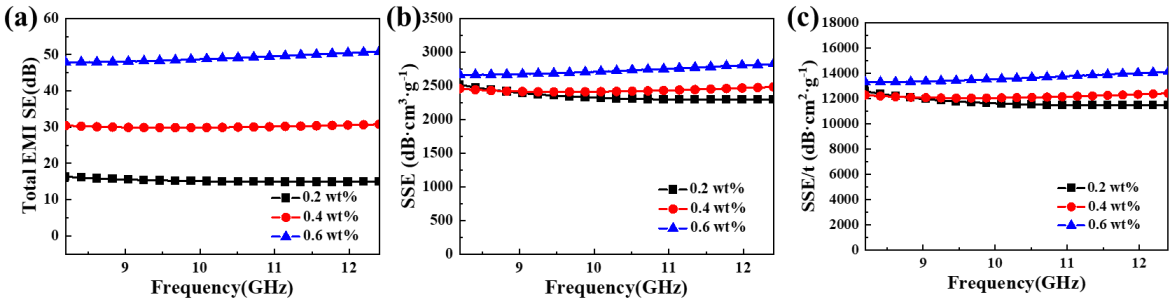

Figure S12. (a) EMI SE, (b)SSE and (c)Absolute EMI SE of GA-T4(LGA) with difference density.

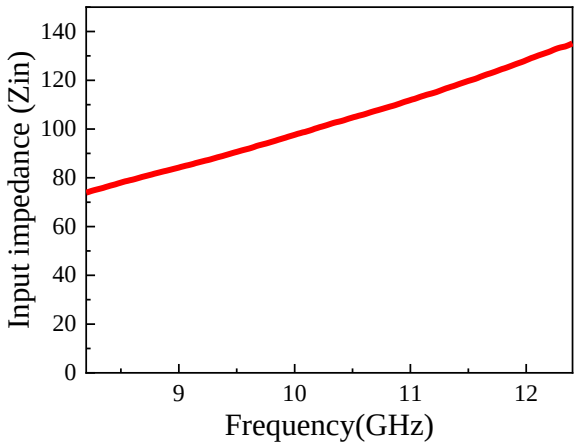

Figure S13. The absorbent input impedance of the GA-T4(LGA) with the thickness of 2mm.

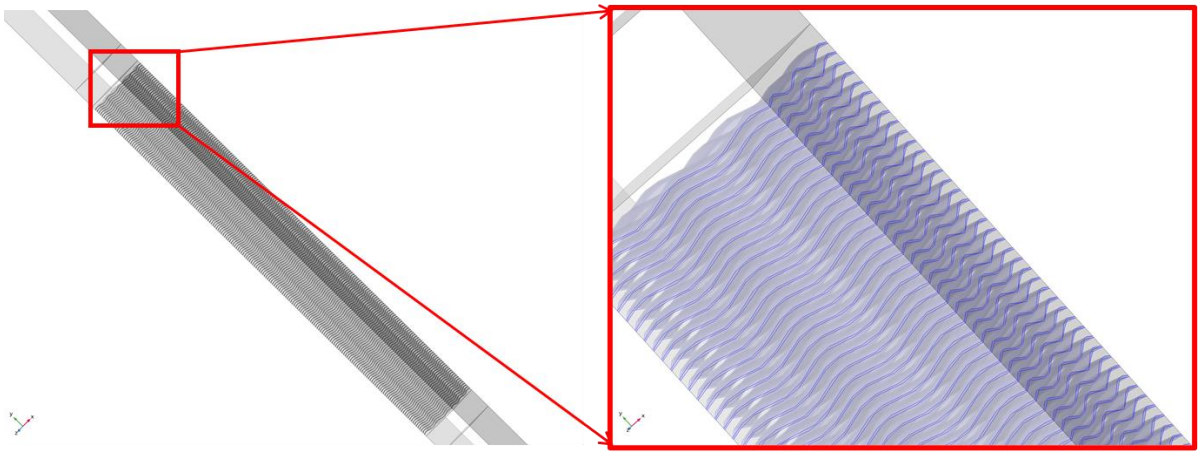

Figure S14. Geometric model used in electromagnetic shielding simulation.

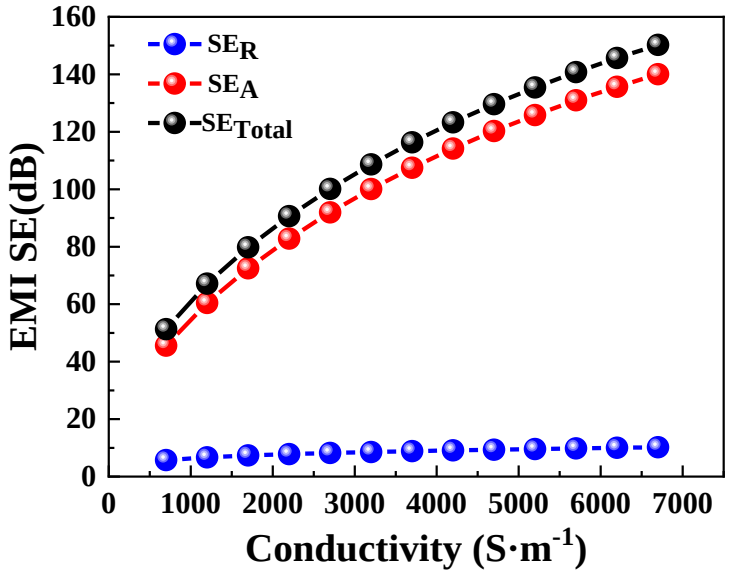

Figure S15. Simulated total shielding effectiveness (SE_{Total}), absorption shielding effectiveness (SE_A), and reflective shielding effectiveness (SE_R) of LGA with different conductivity.

Table S2 Comparison of electromagnetic interference shielding performance for various

materials	Thickness (mm)	EMI SE （dB）	Conductivity (S/m)	Density (g/cm3)	SSE （$dB \cdot cm^3 g^{-1}$）	SSE/t （$dB \cdot cm^2 g^{-1}$）	refs
PEI/graphene form	2.3	13.2	2.2*10-3	0.3	44	191.3	[3]
PI/RGO/MWCNTs foam	0.5	16.6-18.2	1.87	0.44	37.7	754.5-827.3	[4]
PU/RGO foam	20–60	12.4-34.7	0.25	0.027	459	76.5-642.6	[5]
PMMA/graphene foam	2.4	19	3.11	0.79	24	100.21	[6]
porous PS/graphene composite	2.5	17.3/29.3	0.22/1.25	0.27/0.45	63/64.4	256.3/260.4	[7]
PI/rGO foams	0.8	17-21	0.8	0.28	60.7-75	758.9-937.5	[8]
PS/graphene composite	2.5	≈45.1	43.5	1.04	43.4	173.5	[9]
Melamine/tpu/go	2	35.6	45.2	0.21	169	845	[10]
cellulose/go foam	0.6	49.5	91.2	0.596	83	1384.2	[11]
Graphene/PDMS	3	36	200	0.06	600	2000	[12]
graphene/silver nanowires	5	45.2	0.3	0.019	.2379	4757.9	[13]
Phenolic resin/graphene aerogels	4	35	95	0.0143	2447.26	6118.9	[14]
graphene/epoxy composite	4	32	980	1.15	28	69.6	[15]
graphene aerogel-Carbon texture	3	37	——	0.07	528.6	1762	[16]
GA-T0	2	24.5	191	0.0152	1611	8059	This Work
GA-T2	2	41.4	551	0.0185	2238	11189	This Work
GA-T4	2	50.8	705	0.0180	2822	14111	This Work

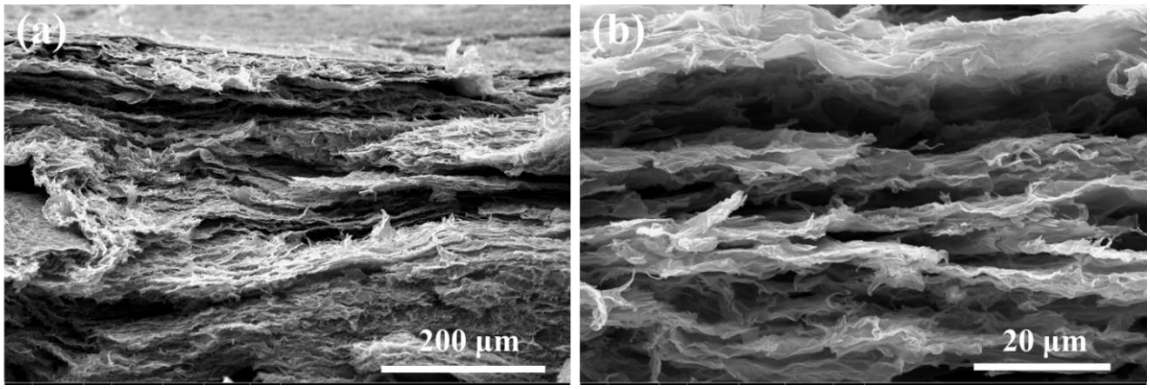

Figure S16. SEM images of GOA-T4 internal morphology after 100 compression cycles.

Table S3 Comparison of Piezoresistive Performance for various materials

materials	preparation method(mm)	compressive strain or pressure range	sensitivity (ΔR/R0 or GF)	response time	refs
graphene form	freeze-drying	0–60%	GF = 1.3	260 ms	[17]
graphene/amorphous carbon hierarchical foam	chemical vapor deposition (CVD)	0–50%	Δ R/R0 = −39% (GF = −7.9)	N/A	[18]
PDMS Foam Coated with Graphene	direct template method	0–70 kPa	0.23 kPa^{-1}	N/A	[19]
graphene/carbon nanotube hybrid foams	freeze-drying	0–80%	GF =6.84	N/A	[20]
carbon black/graphene nanoplatelets-silicone rubber	layer-by-layer (LbL) assembly	0–80%	0.38 kPa^{-1}	N/A	[21]
natural-wood-derived carbon sponge	chemical treating and freeze-drying	0–80%	N/A	N/A	[22]
Cu nanowire aerogel	freeze-drying	0–60%	0.02–0.7 kPa^{-1}	80	[23]
MXene/rGO aerogel	freeze-drying	0–3.5 kPa	4.05 kPa^{-1}	200 ms	[24]
Ti3C2TX MXene hydrogels	polymerization	0–90%	GF = 3.15	N/A	[25]
melamine-sponge-derived carbon	carbonization (800 °C)	0–10 kPa	100.29 kPa^{-1}	N/A	[26]
polydimethylsiloxane foam	etching the Ni foam template	0–80%	~0.60 kPa−1 at 0–1 kPa	30 ms	[27]
GA-T4 (LGA)	3D printing	0–80%	GF = 2	39 ms	This Work

References

[1] Y. Matsubara, *Polymer Engineering & Science* **1980**, 20, 716.

[2] a) B. Shen, Y. Li, D. Yi, W. Zhai, X. Wei, W. Zheng, *Carbon* **2017**, 113, 55; b) S. M. Zhao, Y. H. Yan, A. L. Gao, S. Zhao, J. Cui, G. F. Zhang, *Acs Applied Materials & Interfaces* **2018**, 10, 26723.

[3] J. Ling, W. Zhai, W. Feng, B. Shen, J. Zhang, W. G. Zheng, *Acs Applied Materials & Interfaces* **2013**, 5, 2677.

[4] H. Yang, Z. Yu, P. Wu, H. Zou, P. Liu, *Applied Surface Science* **2018**, 434, 318.

[5] B. Shen, Y. Li, W. Zhai, W. Zheng, *Acs Applied Materials & Interfaces* **2016**, 8, 8050.

[6] H.-B. Zhang, Q. Yan, W.-G. Zheng, Z. He, Z.-Z. Yu, *Acs Applied Materials & Interfaces* **2011**, 3, 918.

[7] D.-X. Yan, P.-G. Ren, H. Pang, Q. Fu, M.-B. Yang, Z.-M. Li, *Journal of Materials Chemistry* **2012**, 22, 18772.

[8] Y. Li, X. Pei, B. Shen, W. Zhai, L. Zhang, W. Zheng, *Rsc Advances* **2015**, 5, 24342.

[9] D.-X. Yan, H. Pang, B. Li, R. Vajtai, L. Xu, P.-G. Ren, J.-H. Wang, Z.-M. Li, *Advanced Functional Materials* **2015**, 25, 559.

[10] B. Fu, P. Ren, Z. Guo, Y. Du, Y. Jin, Z. Sun, Z. Dai, F. Ren, *Composites Part B-Engineering* **2021**, 215.

[11] Z. Guo, P. Ren, Z. Dai, Z. Zong, F. Zhang, Y. Jin, F. Ren, *Cellulose* **2021**, 28, 3135.

[12] Z. Chen, C. Xu, C. Ma, W. Ren, H.-M. Cheng, *Advanced Materials* **2013**, 25, 1296.

[13] X. Liu, T. Chen, H. Liang, F. Qin, H. Yang, X. Guo, *Rsc Advances* **2019**, 9, 27.

[14] Y. Chen, H.-B. Zhang, M. Wang, X. Qian, A. Dasari, Z.-Z. Yu, *Composites Science and Technology* **2017**, 152, 254.

[15] X.-H. Li, X. Li, K.-N. Liao, P. Min, T. Liu, A. Dasari, Z.-Z. Yu, *Acs Applied Materials & Interfaces* **2016**, 8, 33230.

[16] W.-L. Song, X.-T. Guan, L.-Z. Fan, W.-Q. Cao, C.-Y. Wang, M.-S. Cao, *Carbon* **2015**, 93, 151.

[17] J. Kuang, L. Liu, Y. Gao, D. Zhou, Z. Chen, B. Han, Z. Zhang, *Nanoscale* **2013**, 5, 12171.

[18] Y. Ma, M. Yu, J. Liu, X. Li, S. Li, *ACS Applied Materials & Interfaces* **2017**, 9, 27127.

[19] A. Rinaldi, A. Tamburrano, M. Fortunato, M. S. Sarto, *Sensors* **2016**, 16.

[20] J. Li, W. Li, W. Huang, G. Zhang, R. Sun, C.-P. Wong, *Journal of Materials Chemistry C* **2017**, 5, 2723.

[21] Y. Huang, X. Y. He, L. Gao, Y. Wang, C. X. Liu, P. Liu, *Journal of Materials Science-Materials in Electronics* **2017**, 28, 9495.

[22] C. Chen, J. Song, S. Zhu, Y. Li, Y. Kuang, J. Wan, D. Kirsch, L. Xu, Y. Wang, T. Gao, Y. Wang, H. Huang, W. Gan, A. Gong, T. Li, J. Xie, L. Hu, *Chem* **2018**, 4, 544.

[23] X. Xu, R. Wang, P. Nie, Y. Cheng, X. Lu, L. Shi, J. Sun, *ACS Applied Materials & Interfaces* **2017**, 9, 14273.

[24] Y. Ma, Y. Yue, H. Zhang, F. Cheng, W. Zhao, J. Rao, S. Luo, J. Wang, X. Jiang, Z. Liu, N. Liu, Y. Gao, *ACS Nano* **2018**, 12, 3209.

[25] S.-N. Li, Z.-R. Yu, B.-F. Guo, K.-Y. Guo, Y. Li, L.-X. Gong, L. Zhao, J. Bae, L.-C. Tang, *Nano Energy* **2021**, 90, 106502.

[26] W. Liu, N. Liu, Y. Yue, J. Rao, C. Luo, H. Zhang, C. Yang, J. Su, Z. Liu, Y. Gao, *Journal of Materials Chemistry C* **2018**, 6, 1451.

[27] S.-W. Dai, Y.-L. Gu, L. Zhao, W. Zhang, C.-H. Gao, Y.-X. Wu, S.-C. Shen, C. Zhang, T.-T. Kong, Y.-T. Li, L.-X. Gong, G.-D. Zhang, L.-C. Tang, *Composites Part B: Engineering* **2021**, 225, 109243.